International Journal of Solids and Structures 46 (2009) 2750–2756

Contents lists available at ScienceDirect

International Journal of Solids and Structures

journal homepage: www.elsevier.com/locate/ijsolstr

Spatially resolved observations of strain fields at necking and fracture of anisotropic hardened steel sheet material

J. Eman [1], K.G. Sundin *, M. Oldenburg

Solid Mechanics, Luleå University of Technology LTU, SE-97187 Luleå, Sweden

ARTICLE INFO

Article history:
Received 29 October 2008
Received in revised form 28 January 2009
Available online 20 March 2009

Keywords:
Plastic deformation
Strain analysis
Necking
Localization
Mechanical testing
Fracture
Failure analysis
Speckle correlation

ABSTRACT

In this work plastic strain localization, also referred to as necking, of press-hardened ultra-high strength steel is observed using digital speckle correlation. The region of the neck is studied during tensile tests of specimens specially designed to facilitate strain localization at an inner point of the material, thus avoiding edge effects on localization and fracture. By using measurements with a length scale small enough to properly resolve the neck, its growth and shape can be studied. Furthermore, the anisotropy of the material is investigated by examining specimens cut out at different angles to the rolling direction. It is seen that the local fracture strain of specimens cut out along the rolling direction is approximately twice as high as it is for specimens cut out perpendicular to the rolling direction.

1. Introduction

Plastic forming of ductile sheet metal is a very common activity in for example today's automotive industry as well as in other mechanical applications. Also in unintentional situations such as collisions, sheet material is subjected to plastic deformations. In the beginning of the plastic process at low strain levels the state of strain is generally smooth but after this initial stage the developing strain is often localized to a narrow area. This localization is called necking and it is the prelude of fracture because a crack is ultimately formed in the neck. The most well known example of plastic localization is perhaps the forming of a neck towards the end of a standard tensile test.

The localization of strain to a limited region results in a rapidly increasing strain level within this region. This increase in strain will ultimately lead to the onset of fracture which in all practical situations is an unwanted scenario. In many technical applications it is desirable to use the materials to their limits, that is, deform them as much as possible without causing a fracture. Therefore, it is of great interest and importance to widen the knowledge and understanding of the phenomenon of necking.

Within the automotive industry crash-protecting components such as A- and B-pillars, bumper beams and side impact protections are often made from ultra-high strength steel. The purpose is to save weight at maintained or increased structural strength. In order to save even more weight, larger structures of the vehicles could be made from this type of material. However, this development requires a very detailed knowledge of the behaviour of the material, also regarding necking and fracture.

The phenomenon of necking has been studied for a long time. One goal has been to determine the entire true stress–strain relation for a material up to fracture see Zhang and Li (1994), Meuwissen et al. (1998), Zhang (1995), Ling (1996), Koc and Štok (2004), Zhang et al. (1999, 2001a,b) which is of importance for accurate simulation of large-strain applications. In sheet forming processes forming limit diagrams (FLD) are often used to predict local necking and subsequent fracture and the establishment of such diagrams includes study of the necking phenomenon under more general conditions than the conventional uniaxial tensile test. Analytical background for FLD theories can be found in e.g. Hill (1952), Swift (1952), Marciniak and Kuczynski (1967), Storen and Rice (1975), Needleman and Tveergaard (1977) and some recent experimental work is reported in Brunet et al. (1998) and Brunet and Morestin (2001).

Experimental techniques have developed rapidly during the last decade and the trend towards optical field methods is strong. An example of an older experimental work based on conventional microscopic observations of the metallographic structure during deformation is given in Carlson and Bird (1987). Examples of modern methods used in observations of plastic deformation and neck-

* Corresponding author. Tel.: +46 920 491284; fax: +46 920 491047.
E-mail address: kgsundin@ltu.se (K.G. Sundin).
[1] Swerea SICOMP AB, P.O. Box 271, SE-94126 Piteå, Sweden.

0020-7683/$ - see front matter © 2009 Elsevier Ltd. All rights reserved.
doi:10.1016/j.ijsolstr.2009.03.003

ing behaviour are Brunet et al. (1998), Brunet and Morestin (2001), Suprapedi and Toyooka (1997), Gong and Toyooka (1999), Wattrisse et al. (2001a,b), Vial-Edwards et al. (2001), Quinta da Fonseca et al. (2004), Guelorget et al. (2006), Martínez et al. (2003), Labbé and Cordero (2007). It seems that digital speckle correlation (DSC) is perhaps the most commonly used full-field experimental method for studies of plasticity. This is explained by the fact that it has become available even outside optics labs and it is fairly simple to use also by investigators who are not experts in optics. It is also commercially available nowadays. This method is reviewed and evaluated in Tong (2005), Schreier and Sutton (2002), Hild and Roux (2006) and some good examples of its application in material studies can be found in Brunet and Morestin (2001), Quinta da Fonseca et al. (2004), Kajberg and Lindkvist (2004).

DSC is used in the present study with focus on investigation of the nature of necking appearing in ultra-high strength steel under tension. The region of the neck is observed in detail at a number of time instants throughout a tensile test of a specimen. This enables studies of both the growth and the shape of the neck. Strain components in the neck region are recorded during the tensile plastic process. Proper measurements of the necking phenomenon require the length scale of the measurement to be small enough so that the neck is sufficiently resolved. The dependence of different length scales in the measurements is investigated.

In order to investigate the behaviour of the material itself and not the influence from edges, a non-standard specimen shape is developed. The specimen shape is designed to produce plastic strain localization in the centre of the specimen. This causes the fracture to emanate from an interior point of the specimen, thus eliminating influence from edge effects. Also, the chosen specimen design allows the position of the fracture to be determined prior to the experiment and therefore the measurement can be focused to that region, thus enabling a higher spatial resolution.

Anisotropic behaviour regarding plasticity and fracture is common for rolled sheet material and proper understanding and modelling is essential in simulation of sheet forming processes (see Huang et al., 2000; Brunet et al., 2005; Hill, 2001). DSC is a suitable method for experimental investigation of strains in different directions and their development during loading to fracture. Strains at the centre of the neck in specimens taken at 0°, 45° and 90° to the rolling direction are studied in this work. The material in the investigation is a press-hardened ultra-high strength steel.

2. Experiments

2.1. Material and specimens

The material chosen in this investigation is an ultra-high strength steel (hardened 22MnB5) which is used in protective structures in cars. Anisotropy is introduced by the rolling process of the base material. Simultaneous forming and quenching in water-cooled tools gives the material its strength properties. Components may be loaded in such a way that fracture will not emanate from an edge and therefore it is of interest to examine fracture behaviour at an inner point. Conventional tensile specimens (SS EN 10 002-1) with a straight part are unsuitable because the edge may influence the fracture process to a high degree through irregularities, micro cracks and heat effects from the cutting process. Further, the exact position of the final fracture is unforeseeable in such specimens and since local measurement in the area of plastic localisation is the objective of this investigation, straight specimens were not used. Instead a specimen shape with a shallow notch is chosen. A varying cross section of the specimen will cause a non-homogeneous state of strain and stress but the position of the localisation and subsequent fracture is determined by the notch and thus possible to predict with high accuracy.

The suitable shape of the specimens was determined through a pilot study involving FEM-simulations and experimental verification. A plausible stress–strain relation and fracture strain criterion, determined approximately in the study, was used in the simulations and different specimen shapes were tested numerically through simulation of tensile loading to fracture. Shapes leading to localisation and fracture initiation in the inner part of the specimen are potential geometries for this research and specimens with shallow notches showed such behaviour. Lower fracture strain at the edges due to influence from cutting was not assumed in the simulation model and therefore the numerical results had to be verified by a set of preliminary experiments. The final shape of the specimens that was chosen for the rest of the investigation is presented in Fig. 1a.

For reference, conventional tensile tests using straight specimens and an extensometer are performed. There is however a slight modification to the standard straight specimen (SS EN 10 002-1). The sides are not exactly parallel but instead machined with a large radius to ensure that localisation and fracture take place within the gauge length covered by the extensometer. Geometries for both the notched and the straight specimen are presented in Fig. 1.

The conventional tensile testing of straight specimens according to Fig. 1b is performed with an extensometer length of 50 mm. Specimens taken parallel, perpendicular and in a 45° angle to the rolling direction are tested and stress–strain diagrams are presented in Fig. 2. Tests are performed on specimens with thickness t of both 1.2 and 2.4 mm and each test is repeated two times. All specimens are cut from sheets that are hardened in a press between flat cooled surfaces. Abrasive water cutting is used for manufacturing of all the specimens and testing is performed in the as-delivered condition without further treatment.

2.2. Experimental set-up and procedure

Local strains are measured with the method of Digital Speckle Correlation (DSC), which is a multi-point or grid method giving strain data in a large number of points over the monitored area. Speckle patterns in the form of randomly distributed black and white dots were applied to the specimens with spray painting. The experimental arrangement, sketched in Fig. 3, involves a 250 kN servo-hydraulic testing machine (Dartec M1000/RK,

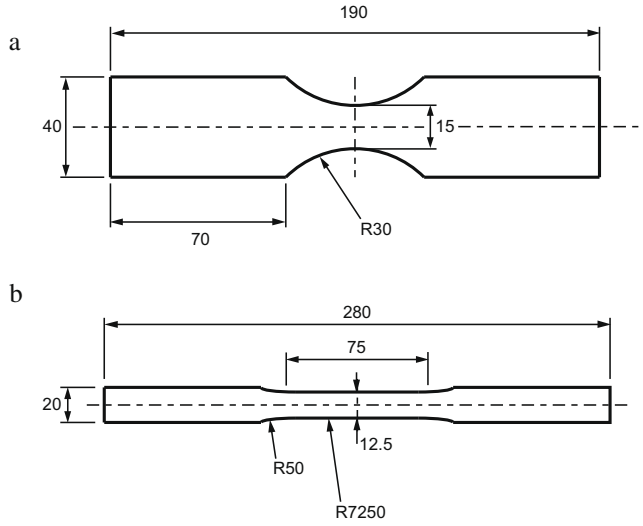

Fig. 1. Specimen shapes (a) with shallow notches and (b) conventional straight specimen.

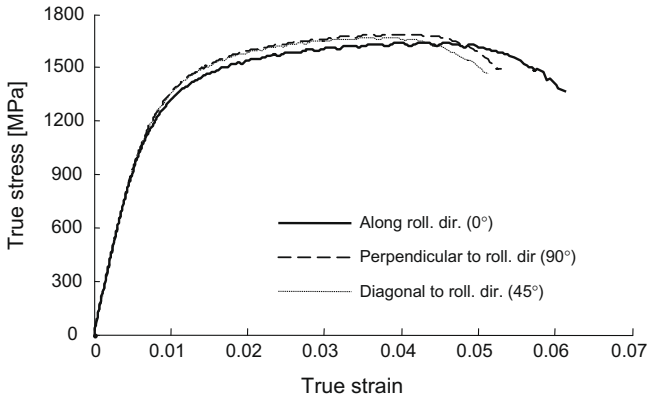

Fig. 2. Stress–strain curves for specimens taken at 0°, 90° and 45° to rolling direction. Sheet thickness t is 1.2 mm.

250 kN) for loading, a CCD camera (PCO Sensicam, 1024×1280 pixels) with a lens (Nikon Micro Nikkor 105 mm) mounted in front of the specimen and an ordinary PC for storing images and evaluating the displacement fields. Two ordinary filament lamps were used for illumination. The camera is fixed to one of the grips of the machine and its lens axis is perpendicular to the specimen plane (x–y-plane). Also an extensometer (Epsilon Technology Corp) with a 50 mm gauge length is used to monitor the elongation of the notched area of the specimen.

The specimen is loaded in prescribed deformation mode in the x-direction at a constant deformation rate of 0.1 mm/s while the framing rate of the camera is two frames per second. A loading sequence to fracture of the specimen takes about 20 s and typically 40 frames are recorded of the translating and deforming speckle pattern at the centre part of the specimen. To acquire an undeformed reference, the framing sequence is started before the tensile deformation starts. The field-of-view is chosen to 5×6mm in order to get a good representation of the developing plastic localisation in the centre of the specimen. As the specimen is stretched, also out-of-plane displacement will occur, especially towards the end of the test when necking takes place at the centre. However, measurements using white light speckles are only moderately affected by out-of-plane displacements and the depth of focus is verified to be sufficient for the application.

For calibration of the spatial resolution of the images a known rigid body displacement (in millimetres) is imposed on the specimen while images are recorded before and after. The displacement field (in pixels) of the images is evaluated and the mean value over each image is used to compute the calibration factor between physical length and number of pixels.

2.3. Evaluation of displacement and strain fields

The displacement fields obtained from the DSC-method are determined by performing a cross correlation procedure on images captured before and after a deformation. The first image is divided into a number of small regions, called sub-images. Each of these sub-images has a unique speckle constellation due to the random pattern on the specimen. The cross correlation procedure searches over the second image and the position where the correlation coefficient for the local speckle pattern is the highest is taken as the new location for the sub-image. From the old and the new positions the displacements can be determined (see Wattrisse et al., 2001a,b; Tong, 2005; Kajberg and Lindkvist, 2004; Sjödahl (1994, 1997)).

It should be noted that the cross correlation procedure used here does not take into account strain or rotation of the sub-images when their new positions are determined. Decorrelation caused by these effects may therefore reduce the accuracy in cases of large strains between the two images. As large total strain levels are of interest in this investigation a sequence of many images with less strain between them is recorded during the process and a stepwise development is determined by repeated use of the correlation procedure on images from the sequence. The output of this procedure is the in-plane displacements u and v of the midpoints of the sub-images for each step in the sequence.

For the determination of the strain state a procedure based on polar decomposition of the deformation gradient is employed. The method is outlined below and the theoretical background can be found in text books such as Holzapfel (2000) and Bonet and Wood (1992). Similar schemes for computation of strains have been used in Wattrisse et al. (2001a,b) and Kajberg and Lindkvist (2004). Generally in a Lagrangian description of deformation we have $\mathbf{x}' = \mathbf{x} + \mathbf{u}(\mathbf{x})$ where $\mathbf{x}'$ is the current position of a particle emanating from the position $\mathbf{x}$ and $\mathbf{u}(\mathbf{x}) = (u(x,y,z)\, v(x,y,z)\, w(x,y,z))$ is the displacement vector. The deformation gradient $\mathbf{F}$ is defined by

$$\mathbf{F} = \frac{\partial \mathbf{x}'}{\partial \mathbf{x}} = \begin{bmatrix} 1+\frac{\partial u}{\partial x} & \frac{\partial u}{\partial y} & \frac{\partial u}{\partial z} \\ \frac{\partial v}{\partial x} & 1+\frac{\partial v}{\partial y} & \frac{\partial v}{\partial z} \\ \frac{\partial w}{\partial x} & \frac{\partial w}{\partial y} & 1+\frac{\partial w}{\partial z} \end{bmatrix} \tag{1}$$

In the present case it is a reasonable assumption that the values of u and v that are measured at the surface of the specimen represent

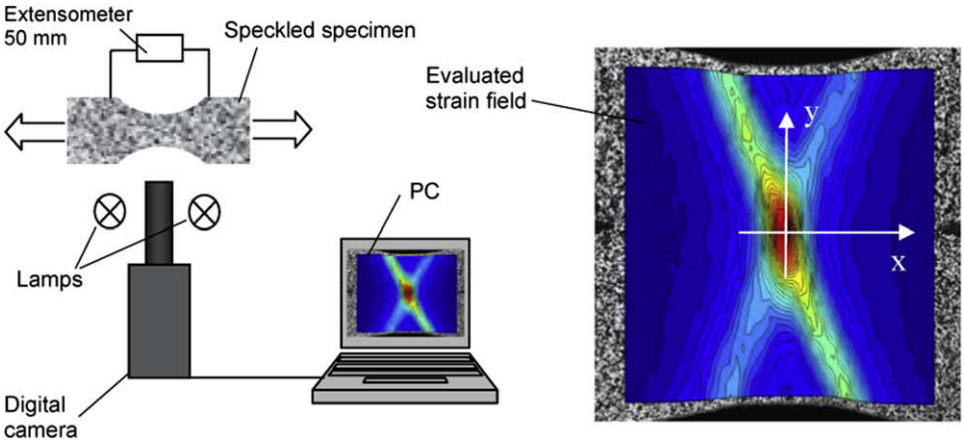

Fig. 3. Experimental setup for tension tests of speckled specimens.

the situation also at the midplane of the sheet implying that u and v are constant through the thickness and thus $\frac{\partial u}{\partial z} = \frac{\partial v}{\partial z} = 0$. Also $w(x,y) = 0$ in the midplane and therefore $\frac{\partial w}{\partial x} = \frac{\partial w}{\partial y} = 0$. The upper left 2×2 matrix of (1) describes the deformation gradient in the x–y-plane and it is denoted $\mathbf{F_{2D}}$. Polar decomposition of $\mathbf{F_{2D}}$ yields

$$\mathbf{F_{2D}} = \mathbf{R_{2D}}\mathbf{U_{2D}} \tag{2}$$

where $\mathbf{R_{2D}}$ is the proper orthogonal rotation tensor ($\mathbf{R_{2D}^T R_{2D}} = \mathbf{I}$) and $\mathbf{U_{2D}}$ is the positive definite and symmetric right stretch tensor $\left(\mathbf{U_{2D}^T} = \mathbf{U_{2D}}\right)$. Then $\mathbf{F_{2D}^T F_{2D}} = (\mathbf{R_{2D}U_{2D}})^{\mathbf{T}}\mathbf{R_{2D}U_{2D}} = \mathbf{U_{2D}^T U_{2D}}$ which is written

$$\mathbf{U_{2D}^2} = \mathbf{F_{2D}^T F_{2D}} \tag{3}$$

Now, spectral decomposition yields

$$\mathbf{U_{2D}} = \lambda_1 \mathbf{n_1 n_1^T} + \lambda_2 \mathbf{n_2 n_2^T} \tag{4}$$

where λ_1 and λ_2 are the square roots of the eigenvalues of the symmetric matrix $\mathbf{U_{2D}^2} = \mathbf{F_{2D}^T F_{2D}}$ and $\mathbf{n}_1$ and $\mathbf{n}_2$ are the corresponding eigenvectors. The logarithmic (Hencky) in-plane symmetric strain matrix $\boldsymbol{\varepsilon_{2D}}$ with components $\varepsilon_x, \varepsilon_y$ and ε_{xy} is then computed as

$$\boldsymbol{\varepsilon_{2D}} = \ln(\mathbf{U_{2D}}) \tag{5}$$

Assuming conservation of volume during plastic deformation, implies $\det \mathbf{F} = 1$ which with Eq. (1) gives

$$\left(1 + \frac{\partial w}{\partial z}\right) \det \mathbf{F_{2D}} = 1 \tag{6}$$

and the normal strain in the thickness direction is then computed as

$$\varepsilon_z = \ln\left(1 + \frac{\partial w}{\partial z}\right) = \ln(\det \mathbf{F_{2D}})^{-1} \tag{7}$$

So, from the DSP-measurements the displacements u and v are known for the experimental nodes corresponding to the midpoints of the subareas. In the next step the in-plane derivatives $\frac{\partial u}{\partial x}, \frac{\partial u}{\partial y}, \frac{\partial v}{\partial x}$ and $\frac{\partial v}{\partial y}$ at each node are calculated approximately in a least square sense by applying a so called first order Savitsky-Golay filter Press et al. (1992). The application of this method is described in Kajberg and Lindkvist (2004) and consists of fitting first degree polynomials for $u(x,y)$ and $v(x,y)$, respectively, to measured displacements of nine (3×3) neighbouring nodes and assigning data for the polynomials (slopes) to the centre node of the 3×3 nodes. Thus approximations of the derivatives are assigned to each experimental node. Next the strain components $\varepsilon_x, \varepsilon_y, \varepsilon_{xy}$ and ε_z are calculated according to Eqs. (1)–(7) and hence the current strains are computed for each experimental node and at each time step. Finally, with the strains known at each time step an equivalent plastic strain can be computed by adding increments according to

$$(\varepsilon_{ep})_n = \sum_{k=1}^{n} (\Delta\varepsilon_{ep})_k = \sum_{k=1}^{n} \left(\sqrt{\frac{2}{3}\left(\Delta\varepsilon_x^2 + \Delta\varepsilon_y^2 + \Delta\varepsilon_z^2 + 2\Delta\varepsilon_{xy}^2\right)} \right)_k \tag{8}$$

where for example $\Delta\varepsilon_x$ is the change in the strain component ε_x between two time steps and n represents the time step for which the computation is performed. Eq. (8) is a discrete version of the von Mises equivalent plastic strain $\varepsilon_{ep} = \int \left(\frac{2}{3} d\varepsilon_{ij}^p d\varepsilon_{ij}^p\right)^{1/2}$. It is an approximation in that out-of-plane shear components are assumed to be negligible which has been verified by FE-calculations in a similar situation in Kajberg and Lindkvist (2004). Also, the elastic contributions to the computed strains are neglected because they are typically two orders of magnitude smaller than the total strains at fracture. The strains produced by the calculation scheme described above in Eqs. (1)–(7) represent Lagrangian logarithmic strains obtained in the experiments. Therefore, the equivalent plastic strain evaluated according to Eq. (8) corresponds to the so called true strain in a uniaxial case with monotonic tensile loading as in a conventional tensile test. The accuracy of the evaluated quantities is influenced by the accuracy of the correlation procedure and of the approximations in the strain calculations. An assessment of the uncertainties can be found in Kajberg and Lindkvist (2004).

As the framing rate of the digital camera is 2 frames per second during the experiments, fracture will occur at an unknown time instant less than half a second after the last frame in the sequence of some 40 images recorded during about 20 s. The strain state at the last frame is taken as representative for fracture and its maximum value defines the value of fracture strains presented below.

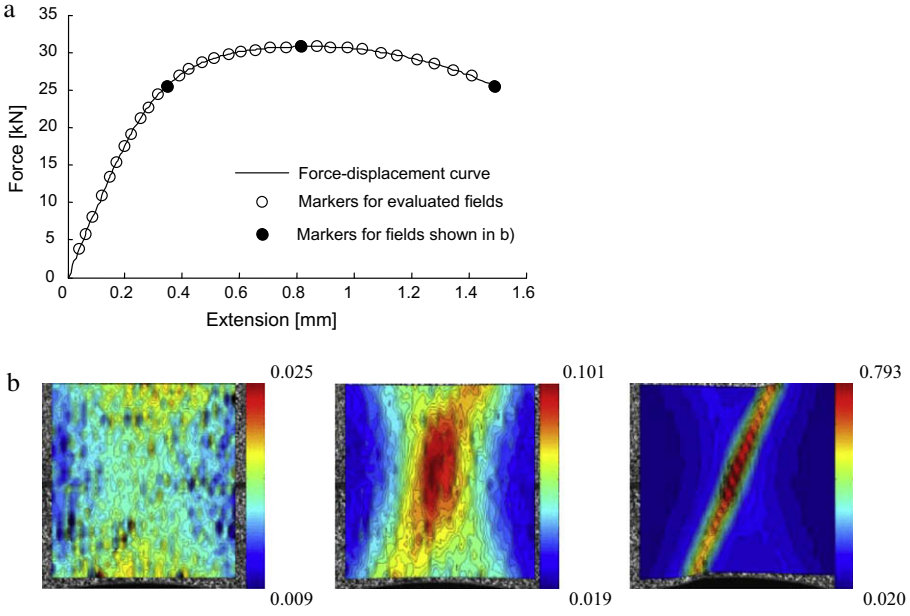

Fig. 4. (a) Force versus extension (b) Normalized strain fields (ε_{ep}) at three time instants.

3. Results

Primary results from the experiments are the time-histories of the tensile force measured by the force transducer, the time-histories of the extension measured by the extensometer and also the digital records of the speckled specimens taken at known time instants with equal intervals. An example of a plot of force versus extension with marked instants for the photographic records is shown in Fig. 4a. From the speckle records the evaluation procedure briefly described above produces information of in-plane displacements (u, v) and of the strains $(\varepsilon_x, \varepsilon_y, \varepsilon_{xy}, \varepsilon_z$ and $\varepsilon_{ep})$ at different time instants during the plastic process. The experimental grid is defined by the chosen midpoints of the sub-surfaces, and strains are evaluated and presented at those points. A time-sequence of plots of for example equivalent plastic strain is produced and an example of three plots from such a sequence is shown in Fig. 4b where the spatial distribution of ε_{ep} (normalized with the fracture strain for 1.2 mm and 0°) according to Eq. (8) is presented. These developing strain fields are studied in order to gain knowledge of the evolution of the necking process.

First a study was performed with the intention to determine the spatial resolution necessary for observation and measurement of the inhomogeneous plastic strain associated with onset and progress of necking in the sheet material of interest. Different distances between sub-surface midpoints, defining the experimental length scale, were used in the evaluation algorithm and the equivalent plastic strain ε_{ep} (Eq. (8)) was calculated. Fig. 5 shows profiles of ε_{ep} along the centreline of the specimen (x-axis) at the last frame before fracture. The eight profiles in each diagram in Fig. 5a and b are evaluated with different spatial resolutions. Due to experimental uncertainty and the numerical differentiation involved in the evaluation process, noise is introduced in the strain data and the noise level increases with a decreasing experimental length scale. An optimum experimental length scale giving sufficient resolution but limited noise is sought and it is concluded from Fig. 5a and b that an experimental length scale of 25 and 50 pixels, respectively, corresponding to about t/10 (t is sheet thickness) renders a sufficiently good representation of the main features of the necking without introducing too much noise. The noise level for the resolution 25 pixels is estimated to less than 0.03 in the normalized strain scale according to Kajberg and Lindkvist (2004). Curves for smaller resolutions than 25 and 50 pixels, respectively, were left out in the presentation to improve clarity in Fig. 5. The resolutions 25 and 50 pixels are used in all subsequent results. In Fig. 5c the normalised strain profiles for both thicknesses are plotted in the same diagram versus the normalised x-coordinate for the experimental length scale $t/10$. The profiles are similar which indicates that the sheet thickness is the dominant length scale in the necking process.

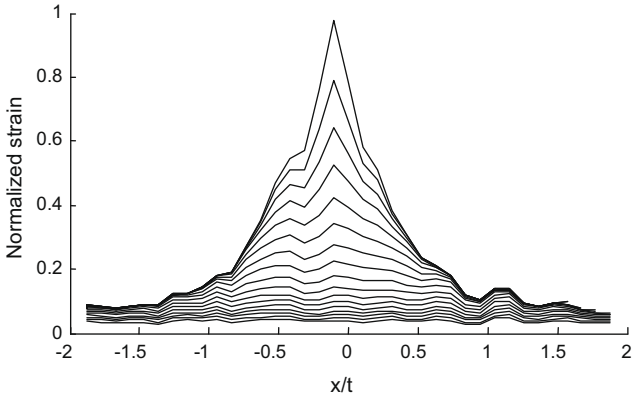

Fig. 6. Strain profiles (ε_{ep}) through the localising area at different times. Thickness is 1.2 mm.

Table 1
Normalized fracture strains.

Specimen	0°	45°	90°
1.2 mm # 1	0.988	1.026	0.651
1.2 mm # 2	1.012	0.992	0.512
1.2 mm, mean	**1.000**	1.01	0.58
2.4 mm # 1	0.931	0.715	0.414
2.4 mm # 2	0.748	0.723	0.323
2.4 mm, mean	0.84	0.72	0.37
Conv 1.2 mm, mean	0.087	0.079	0.076
Conv 2.4 mm, mean	0.112	0.109	0.096

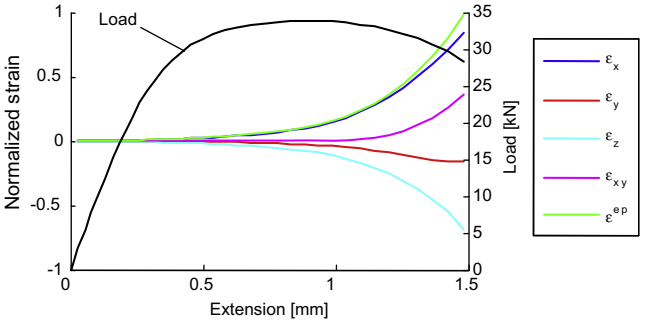

Fig. 7. Load and normalised in-plane strain components versus measured extension.

The development of local strain with time during a tensile test can now be studied using the suitable spatial resolution $t/10$. In Fig. 6, a time-sequence of strain profiles (ε_{ep}) along the x-axis is presented for the 1.2 mm thickness.

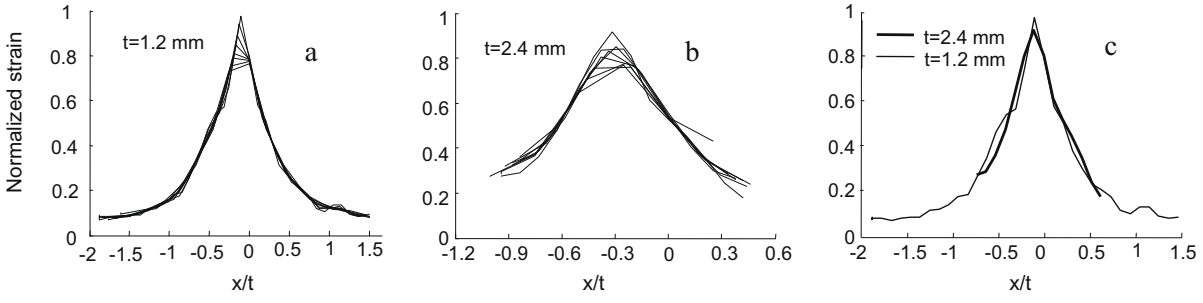

Fig. 5. Strain distribution (ε_{ep}) at the last frame before fracture for different experimental resolutions. (a) 1.2 mm thickness, 25–60 pixels (b) 2.4 mm thickness, 50–120 pixels (c) both thicknesses, 25 and 50 pixels, respectively, corresponding to about $t/10$.

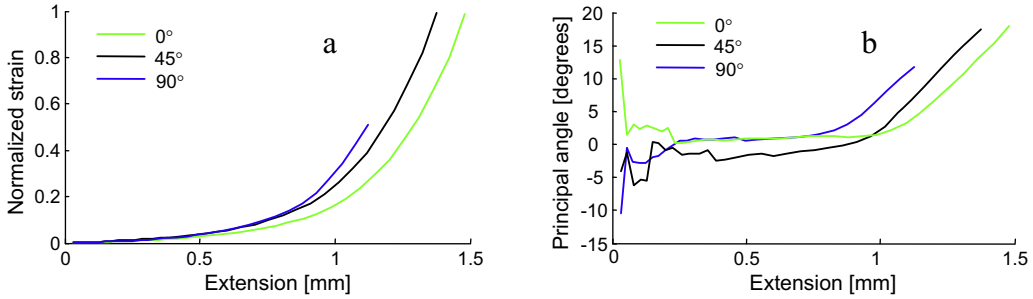

Fig. 8. (a) Normalised effective plastic strains and (b) principle angle versus measured extension for 0°, 45° and 90°. Thickness is 1.2 mm.

One can observe from the strain profiles in Fig. 6 that the localisation has a length scale of about $2t$ at the early stage but that the subsequent development of strain concentrates to the centre part of the localised area. At the last observation before fracture the strain (ε_{ep}) reaches its largest measured value. This maximum value for the 1.2 mm material in the 0° direction is used for normalisation of strains.

It is important to choose a suitable experimental length scale in order to study the spatial features of the necking process but it is also essential to recognise that the evaluated fracture strain will depend on the chosen experimental length scale. It can also be noted that the necking ultimately ends with the formation of one or more cracks at a very small area and the experimental length scale needed to study details of the actual crack formation is of course very small.

Results such as those presented in Fig. 6 are produced for all combinations of the two thicknesses and the three directions. Two repetitions of each experiment were made and normalized values of measured fracture strains are presented in Table 1. Also, in the lower part of Table 1, mean values of the fracture strains for the conventional tensile tests measured with a 50 mm extensometer are presented for comparison. The same normalising value has been used for both the local and the conventional measurements.

The value of the fracture strain is generally largest in the rolling direction and least in the 90° direction. The relations between the results for different directions are more differing for the locally measured strains than for the conventionally measured strains. This is an effect of the much smaller length scale in the case of locally measured strains. The local strains in Table 1 represent an experimental length scale of $t/10$ while the conventional strains represent length scales of $42t$ and $21t$, respectively.

The values in Table 1 reflect the situation at the last frame before fracture at the point where the failure will start before the next picture is taken. These values approximate the fracture strains and are of great interest in for example design work in that they can be used to establish strain based fracture criteria in FEM-simulations with larger length-scales (element sizes). Also, with this sequential field method in combination with the specimen design giving fracture at a predicted inner point, it is possible to follow the development of certain quantities at the critical point where the fracture originates through the plastic process. In Fig. 7 normalised strains $\varepsilon_x, \varepsilon_y, \varepsilon_{xy}, \varepsilon_z$ and ε_{ep} at the fracture point (for 1.2 mm and 0°) are plotted as functions of the extension of the 50 mm extensometer during a test. Also the applied external load F is plotted.

It is obvious from the curves in Fig. 7 that the strain levels at the fracture point increase slowly in the early stages of the process but accelerate towards the end. This is caused by the localisation of the strain field towards the centre of the specimen, visualised in Fig. 4b. One can also note that the relation between the strains change during the test so that the increase in the shear strain ε_{xy} starts late in the process. The strain in the loading direction, ε_x, is of course the dominating strain component throughout the test. Perpendicular to the loading direction the magnitude of ε_z is about three times larger than that of ε_y implying a faster decrease in the thickness direction. This is explained by the geometrical constraint that the notch causes in the y-direction. At the very end the magnitude of ε_y seems to become almost constant which is interpreted as the onset of the final stage in the localizing process when the thinning and the other in-plane strains accelerate towards fracture in the centre of the specimen.

The strains shown in Fig. 7 are, in a sense, the main results of the experiments. However, from these also other quantities can be computed and analysed for the developing plastic process. In general, strain in any direction in the x–y plane can be calculated and in particular the principal strains in the x–y plane and the principal angle may be of interest. Since the strain state is known at different time instants during the plastic deformation it is also possible to evaluate and study rates of all quantities simply by time differentiation.

Some typical results for specimens taken in different angles to the rolling direction are shown in Fig. 8. The development of the equivalent plastic strain in the point of maximum strain for the three directions is shown in Fig. 8a. It is obvious that the strain level at a specific value of the extension is lower for loading in the parallel direction than for the other directions. It is also clear that the fracture strain for loading perpendicular to the rolling direction is much lower than for the other two directions. In Fig. 8b the development of the principle angle in the sheet plane is presented for the different loading directions. The principle angle is almost zero at the beginning of the tensile test but a deviation occurs later. This deviation is synchronous with the development of a preferred shear direction and it occurs earlier for the 90° direction than for the other directions. It is also noted that the principle angle at fracture is smaller for 90° than for 0° and 45°.

4. Conclusions and discussion

A tensile specimen for sheet material testing has been designed to have plastic localisation and onset of fracture at an inner point, thus avoiding influence from cut edges on the fracture process. The shape is of dog-bone type but with shallow notches and therefore the strain state is not homogeneous so an optical field method is utilized for monitoring of the developing strain state. From a sequence of digital photographs of the speckled specimen surface strains are computed at experimental nodes and at times when photographic records are taken. Hence, the measurements allow monitoring of the strain development both in space and in time.

Specimens of ultra-high strength steel sheets, 1.2 and 2.4 mm thick, are cut in 0°, 45° and 90° to the rolling direction by abrasive water cutting. The development of necking, or plastic localization, is studied during deformation. First it is concluded that a spatial

resolution of about $t/10$ is necessary in order to observe the main features of the neck geometry and that the plastic localization gets narrower towards the end of the process. At the last time steps before fracture the increase in strain is concentrated to the central part of the neck with an extension of about half the thickness while the peripheral part of the neck that was active in the earlier stage of the plastic process is not active towards the end. Further it is observed that the locally measured fracture strain is significantly higher for specimens cut out at 0° and 45° to the rolling direction compared to the ones cut out perpendicular to this direction.

The method of digital speckle correlation produces displacement fields from which strain measures of good accuracy are determined. This accuracy could however be improved even further by applying smaller speckles and using a camera with higher resolution. By doing this the spatial resolution of the experiment could be increased compared to the one used in this work. Instead of using a camera with a higher resolution one could use a stronger lens, this is however not trivial since the depth of field then is reduced. The out-of-plane displacement of the surface in the region of the neck might then cause the camera to loose its focus. Even in the measurements carried out in this work the definition of the images is reduced in the region of the neck towards the end of the tensile tests.

The material used for the investigations in this work is only studied in room temperature. In hot-forming operations the blanks are heated to about 900 °C which completely alters the properties of the material. The phenomena of necking and fracture are of great importance in hot-forming operations which is why a natural extension to this work would be to investigate the plastic strain localisation in material at 900 °C.

Acknowledgements

The work presented in this paper is a cooperation between Solid Mechanics at Luleå University of Technology, Sweden, Gestamp R&D in Luleå and Ford Forschungszenter in Aachen Germany. Economic funding is provided by VINNOVA (Swedish Governmental Agency for Innovation Systems), Project P25974-1, and a research grant from Ford URP programme. The authors are grateful to Dr. Daniel Berglund and Dr. Horst Lanzerath for advice during the work and to Mr. Jan Granström for help with the experimental work.

References

Bonet, J., Wood, R.D., 1992. Nonlinear Continuum Mechanics for Finite Element Analysis. Cambridge University Press, Cambridge.

Brunet, M., Mguil, S., Morestin, F., 1998. Analytical and experimental studies of necking in sheet metal forming processes. J. Mater. Process. Technol. 80-81, 40–46.

Brunet, M., Morestin, F., 2001. Experimental and analytical necking studies of anisotropic sheet metals. J. Mater. Process. Technol. 112, 214–226.

Brunet, M., Morestin, F., Walter-Leberre, H., 2005. Failure analysis of anisotropic sheet-metals using a non-local plastic damage model. J. Mater. Process. Technol. 170, 457–470.

Carlson, JM., Bird, JE., 1987. Development of sample-scale shear bands during necking of ferrite–austenite sheet. Acta Metall. 35, 1675–1701.

Hill, R., 1952. On discontinuous plastic states, with special reference to localized necking in thin sheets. J. Mech. Phys. Solids 1, 19–30.

Koc, P., Štok, B., 2004. Computer-aided identification of yield curve of a sheet metal after onset of necking. Comp. Mater. Sci. 31, 155–168.

Gong, XL., Toyooka, S., 1999. Investigation on mechanism of plastic deformation by digital speckle pattern interferometry. Exp. Mech. 39, 25–29.

Guelorget, B., François, M., Vial-Edwards, C., Montay, G., Daniel, L., Lu, J., 2006. Strain rate measurement by electronic speckle interferometry: a new look at the strain localization onset. Mat. Sci. Eng. A 415, 234–241.

Hild, F., Roux, S., 2006. Digital image correlation: from displacement measurement to identification of elastic properties – a review. Strain 42, 69–80.

Hill, R., 2001. On the mechanics of localized necking in anisotropic sheet metals. J. Mech. Phys. Solids 49, 2055–2070.

Holzapfel, GA., 2000. Nonlinear Solid Mechanics – A Continuum Approach for Engineering. John Wiley and Sons Ltd, Chichester.

Huang, H-M., Pan, J., Tang, SC., 2000. Failure prediction in anisotropic sheet metals under forming operations with consideration of rotating principal stretch directions. Int. J. Plast. 16, 611–633.

Kajberg, J., Lindkvist, G., 2004. Characterisation of materials subjected to large strains by inverse modelling based on in-plane displacement fields. Int. J. Solids Struct. 41, 3439–3459.

Labbé, F., Cordero, RR., 2007. Detecting the beginning of shear band formation in uniaxial tensile tests by out-of-plane displacement measurements. Opt. Laser. Eng. 45, 153–159.

Ling, Y., 1996. Uniaxial true stress–strain after necking. AMP J. Technol. 5, 37–48.

Marciniak, Z., Kuczynski, K., 1967. Limit strains in the process of stretch forming sheet metals. Int. J. Mech. Sci. 9, 609–620.

Martínez, A., Rodríguez-Vera, R., Rayas, JA., Puga, HJ., 2003. Fracture detection by grating moiré and in-plane ESPI techniques. Opt. Laser. Eng. 39, 525–536.

Meuwissen, MHH., Oomens, CWJ., Baaijens, FPT., Petterson, R., Janssen, JD., 1998. Determination of the elasto-plastic properties of aluminium using a mixed numerical–experimental method. J. Mater. Process. Technol. 75, 204–211.

Needleman, A., Tveergaard, V., 1977. Necking of biaxially stretched elastic–plastic circular plate. J. Mech. Phys. Solids 25, 159–183.

Press, W.H., Teukolsky, S.A., Vetterling, W.T., Flannery, B.P., 1992. Numerical Recipes in C, 2nd ed. Cambridge University Press, Cambridge.

Quinta da Fonseca, J., Mummery, P.M., Withers, P.J., 2004. Full-field strain mapping by optical correlation of micrographs acquired during deformation. J. Microsc. 218, 9–21.

Schreier, HW., Sutton, MA., 2002. Systematic errors in digital image correlation due to undermatched subset shape functions. Exp. Mech. 42, 303–310.

Sjödahl, M., 1994. Electronic speckle photography: increased accuracy by nonintegral pixel shifting. Appl. Opt. 33, 6667–6673.

Sjödahl, M., 1997. Accuracy in electronic speckle photography. Appl. Opt. 36, 2875–2885.

Storen, S., Rice, JR., 1975. Localized necking in sheet. J. Mech. Phys. Solids 23, 421–441.

Suprapedi, Toyooka, S., 1997. Time-division observation of plastic deformation process using digital speckle pattern interferometry. Opt. Rev. 4, 284–287.

Swift, W., 1952. Plastic instability under plane stress. J. Mech. Phys. Solids 1, 1–18.

Tong, W., 2005. An evaluation of digital image correlation criteria for strain mapping applications. Strain 41, 167–175.

Vial-Edwards, C., Lira, I., Martinez, A., Münzenmayer, M., 2001. Electronic speckle pattern interferometry analysis of tensile tests of semihard copper sheets. Exp. Mech. 41, 58–62.

Wattrisse, B., Chrysochoos, A., Murracciole, J-M., Nemoz-Gaillard, M., 2001a. Analysis of strain localization during tensile tests by digital image correlation. Exp. Mech. 41, 29–39.

Wattrisse, B., Chrysochoos, A., Murracciole, J-M., Nemoz-Gaillard, M., 2001b. Kinematic manifestations of localisation phenomena in steels by digital image correlation. Eur. J. Mech. A/Solids 20, 189–211.

Zhang, KS., 1995. Fracture prediction and necking analysis. Eng. Fract. Mech. 52, 575–582.

Zhang, ZL., Hauge, M., Ødegård, J., Thaulow, C., 1999. Determining material true stress–strain curve from tensile specimens with rectangular cross-section. Int. J. Solids Struct. 36, 3351–3497.

Zhang, KS., Li, HZ., 1994. Numerical analysis of the stress–strain curve and fracture initiation for ductile material. Eng. Fract. Mech. 49, 235–241.

Zhang, ZL., Ødegård, J., Søvik, OP., 2001a. Determining true stress–strain curve for isotropic and anisotropic materials with rectangular tensile bars: method and verifications. Comp. Mater. Sci. 20, 77–85.

Zhang, ZL., Ødegård, J., Søvik, OP., Thaulow, C., 2001b. A study on determining true stress–strain curve for anisotropic materials with rectangular tensile bars. Int. J. Solids Struct. 38, 4489–4505.